

Effects of fetal position on the loading of the fetal brain during the onset of the second stage of labour

Alice M. Collier^a, Erin Louwagie^b, Ghaidaa A. Khalid^{c,d}, Mike D. Jones^{c,*},
Kristin Myers^{b,*}, Antoine Jerusalem^{a,*}

^a*Department of Engineering Science, University of Oxford, Oxford, UK*

^b*Department of Mechanical Engineering, Columbia University, New York, NY, USA*

^c*School of Engineering, Cardiff University, Cardiff, UK*

^d*Middle Technical University, Electrical Engineering Technical College, Baghdad, Iraq*

Abstract

During vaginal delivery, the delivery requires the fetal head to mold to accommodate the geometric constraints of the birth canal. Excessive molding can produce brain injuries and long-term sequelae. Understanding the loading of the fetal brain during the second stage of labour (fully dilated cervix, active pushing, and expulsion of fetus) could thus help predict the safety of the newborn during vaginal delivery. To this end, this study proposes a finite element model of the fetal head and maternal canal environment that is capable of predicting the stresses experienced by the fetal brain at the onset of the second phase of labour. Both fetal and maternal models were adapted from existing studies to represent the geometry of full-term pregnancy. Two fetal positions were compared: left-occiput-anterior and left-occiput-posterior. The results demonstrate that left-occiput-anterior position reduces the maternal tissue deformation, at the cost of higher stress in the fetal brain. In both cases, stress is concentrated underneath the sutures, though the location varies depending on the presentation. In summary, this study provides a patient-specific simulation platform for the study of vaginal delivery and its effect on both the fetal brain and maternal anatomy. Finally, it is suggested that such an approach has the potential to be used by obstetricians to support their decision-making processes through the

*Corresponding authors: jonesmd1@cardiff.ac.uk; kmm2233@cumc.columbia.edu; antoine.jerusalem@eng.ox.ac.uk

simulation of various delivery scenarios.

Keywords: finite element, simulation, labour, fetal head molding

2010 MSC: 00-01, 99-00

1. Introduction

The fetal skull is comprised of plates of cranial bone separated by membranous connective tissues called sutures and fontanelles [1]. During vaginal delivery, the fetal head deforms, accommodated by the movements of these cranial bones, to adapt to the geometry of the maternal birth canal [2, 3]. This is commonly referred to as fetal head molding. Typically, the frontal and occipital bones are compressed inwards and the parietal bones are displaced up and outwards, reducing the suboccipitobregmatic diameter, the diameter of the head that passes through the canal, by about 1 cm [4]. This also causes a change in shape of the brain [5].

During birth, the fetus can sustain injury or birth trauma. The prevalence of birth trauma in spontaneous vaginal birth is 1.42% [6, 7]. The majority of these birth traumas occur during transit through the birth canal and most stem from excessive molding of the fetal skull [4, 6, 7, 8, 9]. Excessive molding can occur if the fetus is malpositioned, labour is prolonged, or if contractions are strong [8]. This can cause extra- and intracranial lesions, which can lead to hemorrhages, which in turn can cause long-term sequelae, such as hydrocephalus, seizure disorders or intellectual/developmental disorders [4, 9]. Although the majority of these birth traumas occur during transit through the birth canal, cesarean delivery does not necessarily alleviate all delivery risks. Indeed, cesarean itself is a non-straightforward operation with a higher incidence of morbidity and mortality, especially if vaginal delivery has already begun [10, 11]. The fetus being often removed head first, it is not either a load-free procedure for the head [10, 11]. Understanding the factors that influence fetal head molding and the compression of the brain during vaginal delivery is thus still required to understand and prevent fetal brain injury.

27 Occiput anterior is the most common and safest fetal position during labour.
28 The second most common presentation is occiput posterior [12]. Persistent
29 occiput posterior, when the fetal head does not rotate before or during labour
30 to the anterior position, is associated with worse fetal and maternal outcomes
31 [13, 14, 15]. Investigating the mechanics and loading of the fetal head would
32 help elucidate why one position has less favorable outcomes.

33 Due to the practical constraints of studying birthing mechanics in vivo, com-
34 putational approaches have provided key insights into the mechanics of fetal
35 head molding. In 1980, McPherson and Kriewall [16] used finite element (FE)
36 modeling to investigate the deformation of the pre-term and term parietal bones
37 during birth. They established pre-term parietal bones deform two to four times
38 more than at term, thus suggesting increased deformation of the pre-term skull
39 could be why premature birth is the one most significant risk factors in neonatal
40 death. In 2001, Lapeer and Prager [17] used FE modeling to propose a non-
41 linear static model of a fetal skull subjected to intrauterine and head-to-cervix
42 pressures during the first stage of labour, when involuntary uterus contractions
43 and cervix dilating to full dilation is evident [6]. The deformation of their
44 model showed good agreement with clinical experiments. Pu et al. [18] also
45 investigated the effect of intrauterine and head-to-cervix pressures during the
46 first stage of labour. They found that, as labour forces increased, so did the
47 degree of fetal head molding. More recently, Moura et al. and Borges et al.
48 have investigated the effect of fetal head molding on the pelvic floor during the
49 second stage of labour [19, 20, 21]. Their models consisted of the key pelvic floor
50 muscles and ligaments, pelvis, and fetal head (skull, suture, cerebrospinal fluid
51 (CSF), brain). It was found that fetal head molding reduces the stretch on the
52 pelvic floor, maternal position and fetal position both affect pelvic floor damage
53 and fetal head molding, and higher labour pressure and longer duration increase
54 fetal head molding. These studies provide good insight into the potential use
55 of FE analysis for investigating the effect of labour on the fetal head, though
56 their main focus was primarily on the maternal pelvic floor. Although studies
57 have looked at how the brain deforms due to head moulding and investigated

58 changes in intracranial pressure and other metrics during labour, no FE studies
59 have been reported investigating the effect of fetal skull moulding on the stress
60 experienced by the fetal brain [5, 22].

61 In this study, a FE model of a complete fetal head and select maternal organs
62 are used to investigate the influence of fetal head position on the compression
63 of the fetal brain during the onset of the second stage of labour, with active
64 pushing during contractions and a fully dilated cervix [6]. Both the fetal and
65 maternal models are presented, along with the boundary conditions of the FE
66 models. Finally, the results for two fetal presentations are shown and discussed.

67 **2. Methods and Materials**

68 *2.1. Finite element models*

69 *2.1.1. Fetal head model*

70 A simplified fetal head model was created to reduce computational time, the
71 pipeline for which is shown in Figure 1. The simplified fetal head model was
72 created by fitting four ellipsoids to one half of the surface of a high-fidelity fetal
73 head model, and then mirrored to create a symmetric model. The high-fidelity
74 fetal head model was built from segmenting a post-mortem high-resolution com-
75 puter tomography scan data set of a 10 day-old infant head [23, 24]. The fetal
76 head does not increase in size significantly 10-day post-partum but the fetal
77 head model’s biparietal diameter was compared to WHO’s fetal growth charts
78 and found to be within the range of a 37-40 week gestation fetus [25, 26]. The
79 fitted ellipsoids (excluding the jaw) were intersected and smoothed together,
80 and the sutures were then added by mapping the sutures positions from the
81 high-fidelity model onto this surface geometry. The resulting simplified geom-
82 etry was then meshed in ICEM CFD (version 2020 R2, ANSYS, Pennsylvania,
83 USA), and extruded to the average thickness of the original skull, and both
84 CSF layer and brain were meshed in the remaining intracranial space. The
85 resulting fetal head mesh consisted of linear triangular prism and tetrahedral

86 elements and had significantly fewer elements (44,060), compared to the high-
 87 fidelity model (317,121). The simplified fetal head model was then compared
 88 to the original reference fetal head model in MeshLab (version 2022.02, Visual
 89 Computing Lab, ISTI-CNR, Pisa, Italy) by computing the Hausdorff distances
 90 between each vertex on the simplified model to the reference high-fidelity model,
 91 shown in Figure 2 [27, 28]. The model shows good agreement with the high-
 92 est disparities around where the jaw extends from the rest of the skull, as the
 93 simplified model does not have a jaw.

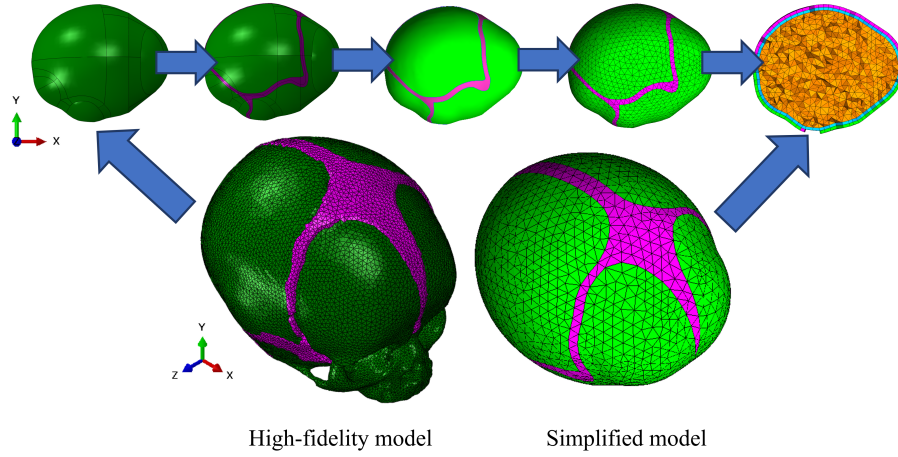


Figure 1: Pipeline for the creation of the simplified fetal head model, from the high-fidelity head model. Green – cranial bones, pink – suture, blue – CSF, and orange – brain.

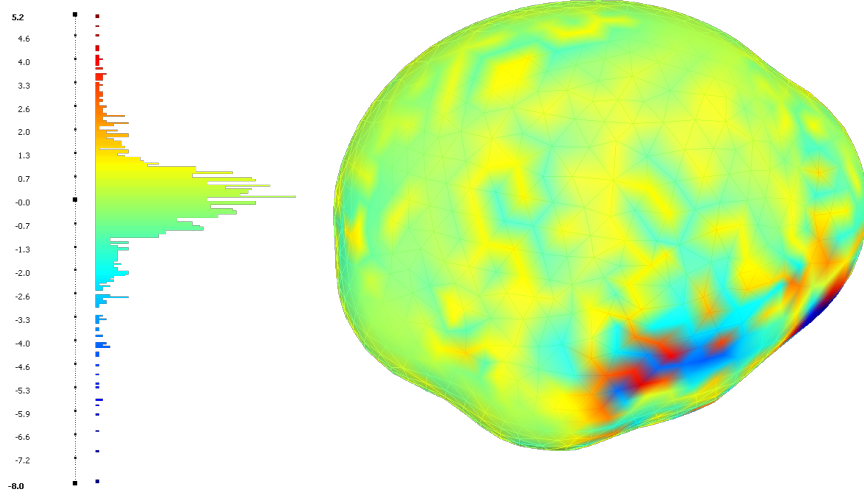


Figure 2: Lateral view of the simplified head and quality histogram, for the distance between the simplified head model and high-fidelity head model. Distance in mm.

2.1.2. Maternal model

The parametric “soft” maternal anatomy, excluding pelvis, was built from a series of ultrasound measurements using a simplistic Boolean geometry method [29]. The original model was intended for pregnancy simulation and adapted for labour for this study. At the onset of labour, the fetal membrane breaks, the amniotic fluid is released, and no longer serves any mechanical purpose [30]. The cervix also softens significantly, progressively dilating from 1 cm to 10 cm in diameter, and shortens, being incorporated into the lower section of uterus [31, 6]. Accordingly, the fetal membrane was removed from the maternal model and the cervix artificially dilated and shortened. In our work, the vaginal canal was reconstructed to provide a more realistic morphology from baseline measurements [32, 33]. To save on computational run time, the upper section of the uterus and abdomen of the original model were discarded. Furthermore, both bladder and bowel are compressed during labour and provide additional softening mechanisms for the enlargement of the vaginal canal. Accordingly,

109 cavities were included in the model to account for those, thus facilitating the
110 descent and minimising the number of distorted elements. This was done using
111 standard shapes and curves in ICEM CFD to approximate the size of the organs
112 in late gestation females from MRI data.

113 The maternal pelvis was built from segmenting MRI data of a pregnant
114 female, and consisted of sacrum, coccyx and hip bones. This was further devel-
115 oped by extending the profile of the sacral promontory to create the “lumbar
116 vertebrae” and the inclusion of the symphysis pubis and other cartilaginous
117 joints of the pelvis, using baseline measurements, for more realistic boundary
118 conditions [34]. The pelvis was then positioned inside the abdomen of the para-
119 metric maternal anatomy. The geometry was then meshed in ICEM CFD, using
120 tetrahedral volume elements. A mesh convergence test was conducted and the
121 final maternal mesh contained a total of 214,122 linear tetrahedral hybrid ele-
122 ments and 40,352 nodes (see Figure 3).

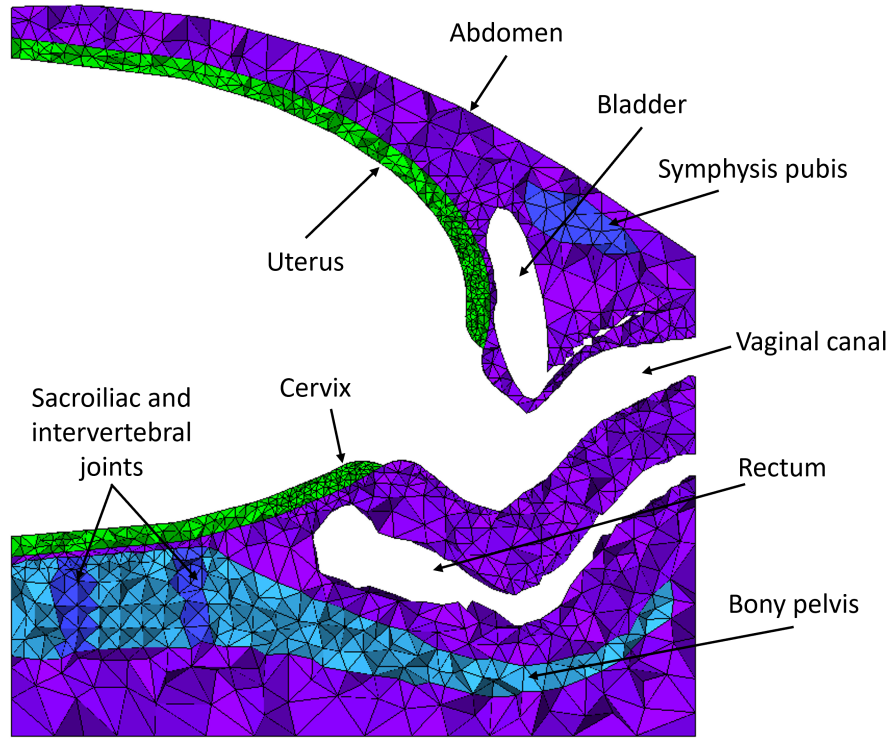


Figure 3: Sagittal view of the FE maternal model.

2.2. Fetal head material properties

2.2.1. Fetal cranial sutures

Few studies exist on the mechanical properties of fetal cranial sutures. Coats and Margulies [35] carried out three-point bending and tension tests, at high strain rates, on samples cut from infant cadavers, of an age range of 21 weeks gestation to one year-old. This is the only study carried out on human neonatal cadavers, therefore this study's data was used as a first approximation. The sutures were modeled as a hyperelastic, nearly incompressible material, using a first order Ogden model, with parameters adapted from the Ogden model used by Li et al. [36], scaling μ_0 down to the modulus of neonatal sutures [35].

133 2.2.2. *Fetal cranial bones*

134 Fetal cranial bone was modeled as orthotropic linear elastic. Pediatric cranial
135 bone is a highly curved and very thin structure, with a visible fiber orientation
136 pattern as spines of bone grow outward from the cranial bones' ossification
137 centers towards the sutures [37, 38].

138 Young's moduli parallel and perpendicular to the fibers of fetal frontal and
139 parietal cranial bone were taken from McPherson and Kriewall's 1980 and 1981
140 studies [37, 39], with values calculated from averaging term data (37 - 42 weeks
141 gestation). Only frontal and parietal bones have been tested at the slow strain
142 rates appropriate for birth loading scenarios. Therefore, the Young's modulus
143 for occipital bone was estimated from the ratio of Young's modulus for occipital
144 to parietal bones at high strain rates (2.015:1) [35].

145 Fiber directions of the FE head model were defined by spherical material
146 orientations, at the ossification centers. The fiber orientations are shown in
147 Figure 4 and material properties are given in Table 1.

148 Note that the lower frontal bones and base of the skull (in lieu of the jaw)
149 were modeled as a rigid body, as shown in blue in Figure 4, as the pushing
150 boundary condition down the vaginal canal was applied by driving the jaw
151 along a chosen direction. This large group of elements was selected to prevent
152 sudden loading of a small number of elements in the fetal head. Additionally,
153 note that this region of the skull is not expected to significantly deform during
154 labour when compared to other tissues.

155 2.2.3. *Brain and CSF*

156 Whilst a large body of literature on the viscoelasticity of the brain exists [40,
157 41], there is significantly less on the fetal/infant brain. Additionally, within the
158 limited literature, there is significant discrepancy between the levels of accuracy
159 of i) the model and ii) the experiments from which they are calibrated [42,
160 43, 44]. Here, as a first approximation the brain was modeled as a nearly
161 incompressible isotropic hyperelastic Ogden material, with parameters from the
162 literature [43]. The CSF was modeled as a nearly incompressible isotropic linear

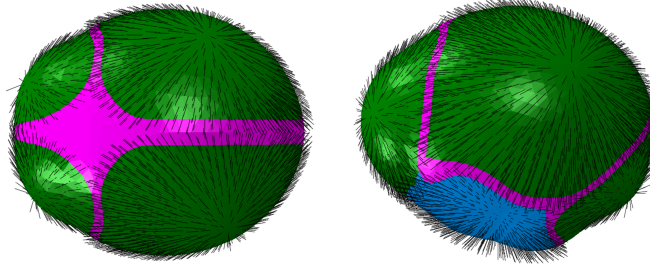


Figure 4: Superior and lateral views of the bone fiber direction on the fetal head model as prescribed by spherical orientations at the bone ossification centers. Green – cranial bones, pink – sutures, blue – rigid part of the fetal jaw and skull base, and black lines – bony fiber directions.

163 elastic material, as adopted by several FE pediatric head simulations [45, 36, 46].
 164 The material properties are given in Table 1.

165 *2.3. Maternal material properties*

166 *2.3.1. Abdomen*

167 The maternal abdomen was modeled as a nearly incompressible isotropic
 168 hyperelastic ne-Hookean material. This is a homogenized model that represents
 169 all the tissues and organs that surround the vaginal canal and uterus, as well
 170 as the added cavities, with parameters typically used in pregnancy and labour
 171 simulations [29, 47] (Table 2).

172 *2.3.2. Uterus and cervix*

173 The uterus and cervix were modelled as one continuous isotropic nearly in-
 174 compressible hyperelastic material. The material properties of the pregnant
 175 uterus were adapted from Manoogian et al. who conducted dynamic uniaxial
 176 tension tests on pregnant human uterus specimens [48]. For this present study,
 177 an Ogden hyperelastic model was fitted to the average true stress-strain curve
 178 extracted from uniaxial tensile tests in this reference, see Figure 5. This was
 179 performed with the MATLAB's (version R2019a, The MathWorks Inc., Mas-
 180 sachusetts, USA) least-square fit function; the resulting parameters are shown

Table 1: Fetal head material properties used in the birth simulation. E , C_0 , σ_y , μ have units MPa, D_1 has units of MPa^{-1} , ρ has units kg/m^3 , and ν and α are dimensionless.

Cranial Bones	Orthotropic linear elastic				
$\rho = 1,896$	E_1	E_2	ν_{12}	ν_{13}	ν_{23}
Frontal	3057	1700	0.190	0.110	0.220
Occipital	2839	472	0.190	0.045	0.220
Parietal	3705	951	0.190	0.045	0.220
Cranial Sutures	Ogden				
$\rho = 1,025$	μ	α	D_1		
	0.0294	6.9	7.0373		
CSF	Linear elastic				
$\rho = 1,000$	E	ν			
	0.00120	0.45			
Brain	Ogden				
$\rho = 997$	μ	α	D_1		
	0.0002957	0.0323	836.65		

181 in Table 2.

182 2.3.3. Pelvis

183 The bony pelvis was modeled as a compressible isotropic linear elastic mate-
184 rial, and the symphysis pubis, sacroiliac, and intervertebral joints were modeled
185 as nearly incompressible isotropic linear elastic materials, with parameters taken
186 from the literature [49, 50], see Table 2.

187 2.4. Head model validation

188 To validate the fetal head FE model, a series of head compression simulations
189 were carried out, and compared against the head compression tests conducted

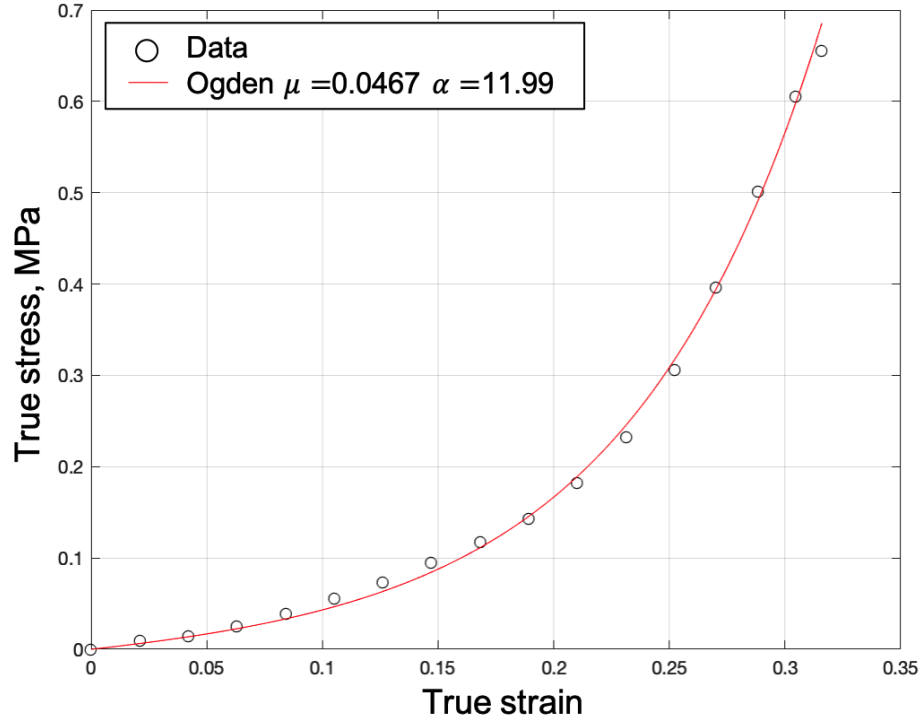


Figure 5: Uterus material model fitted to material test data from Manoogian et al. [48], units in MPa.

190 by Loyd et al. [51]. In this work, fetal head cadavers were compressed in the di-
 191 rection of the biparietal diameter (BPD) and fronto-occipital diameter (FOD),
 192 at several strain-rates. Nodes were kept fixed after contact to avoid rotation
 193 of the head during compression. The quasi-static compressions were simulated
 194 in ABAQUS/Standard (version 6.14-5, Dassault Systems, Paris, France) using
 195 a quasi-static implicit dynamic step. The force-displacement curves from both
 196 compressions are shown in Figure 6. As can be seen, the head model shows an
 197 excellent agreement in both curve shape and magnitude with those measured
 198 by Loyd et al. [51], without the need for any further calibration. The discrep-
 199 ancy in force-displacement evolution in the FOD direction could be explained

Table 2: Maternal tissue material properties used in the birth simulation. E and μ have units of MPa, D_1 has units of MPa^{-1} , ρ has units kg/m^3 , and ν and α are dimensionless.

Abdomen	Neo-Hookean		
$\rho = 1,000$	$C_1 = 0.005$	$D_1 = 20.69$	
Uterus & cervix	Ogden		
$\rho = 950$	$\mu = 0.0467$	$\alpha = 11.99$	$D_1 = 4.27$
Bone	Linear Elastic		
$\rho = 1,890$	$E = 1,100$	$\nu = 0.3$	
Cartilage	Linear Elastic		
$\rho = 1,200$	$E = 5$	$\nu = 0.45$	

by the boundary conditions that Loyd et al. used. Indeed, they allowed for the intracranial content to freely flow out of the cranium during compression, whereas, in our model, the CSF is modelled using solid elements, and as such, cannot flow out of the cranium as a fluid would [51]. This leads to a stiffening of the overall head as compression increases.

2.5. Vaginal delivery simulations

The boundary conditions for the second stage of labour simulation are shown in Figure 8. The cut surface of the maternal model was constrained in all directions and the back surface constrained in the downwards direction. This allowed the mother’s abdomen and the vaginal opening to move freely.

The contact between the fetal head and the internal surfaces of the uterus and vaginal canal was defined using a slave-master contact algorithm. The maternal surface was the slave and the fetal surface was the master as driven by the difference in mesh density. During pregnancy, the baby is coated in a protective layer called the vernix caseosa, which acts as a lubricant during labour [52]. Therefore, tangential contact was defined as frictionless and normal contact was defined as hard.

Two labour scenarios were simulated, the fetus positioned left occiput ante-

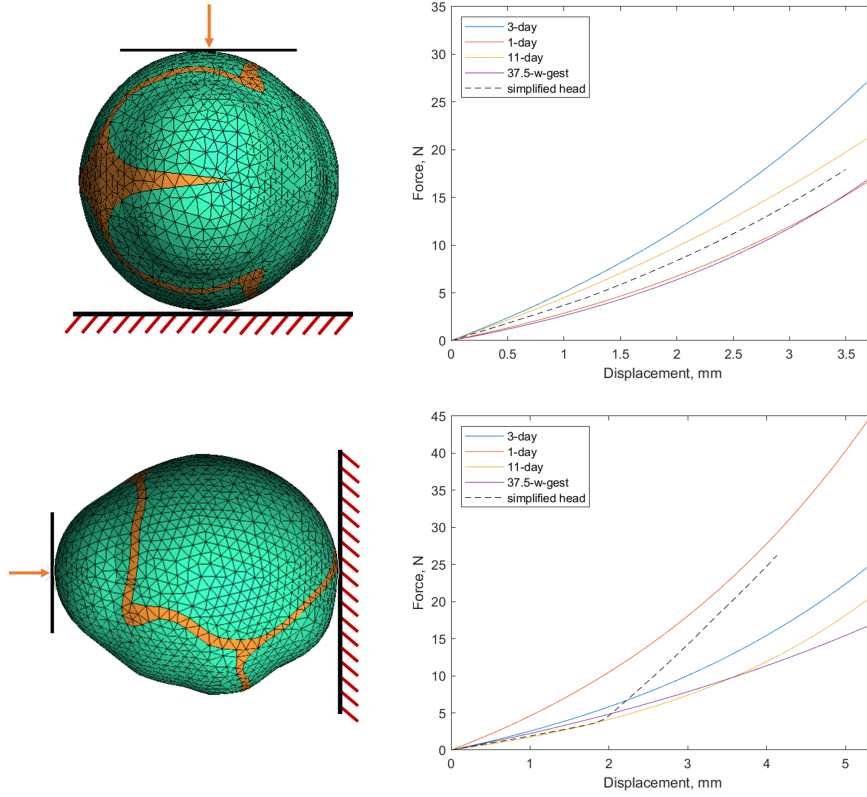


Figure 6: Compression head validation results compared with experimental results [51], top: biparietal compression and bottom: fronto-occipital compression.

rior (LOA) and left occiput posterior (LOP), both presenting vertex. In LOA, see Figure 7a, the fetus is longitudinal, head first, facing the mother's spine, head turned towards the mother's right side, chin tucked into the neck, and with the suboccipitobregmatic diameter to pass through the vaginal canal. In LOP, see Figure 7b, the same as above applies except that the fetus is facing away from the mother's spine head turned towards the mother's right side. Of all the potential positions of the fetus, LOA is the most common and deemed the safest [6].

The simulations were carried out in ABAQUS/Standard, using a dynamic

227 implicit step used under quasi-static loading conditions. To simulate labour,
228 a large group of elements in the fetus' skull base was made rigid and dis-
229 placed along the axis of the vaginal canal, with translations allowed in maternal
230 anterior-posterior direction.

231 The following results were extracted and compared between the two fetal
232 head positions: fetal progression, fetal station, moulding index, von Mises stress
233 and pressure in the fetal brain, change in fetal brain shape, force required to
234 displace the fetal head, and stretch and strain of the maternal tissues.

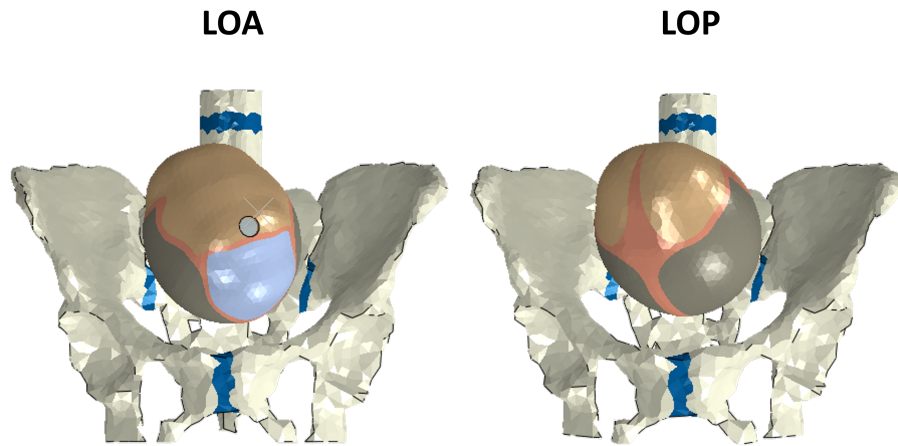


Figure 7: Anterior view of the FE fetal head model positioned LOA (the fetus is longitudinal, head first, facing the mother's spine, head turned towards the mother's right side, and chin tucked into the neck) and LOP (the fetus is facing away from the mothers spine and head turned towards the mother's right side) in the FE maternal pelvis model.

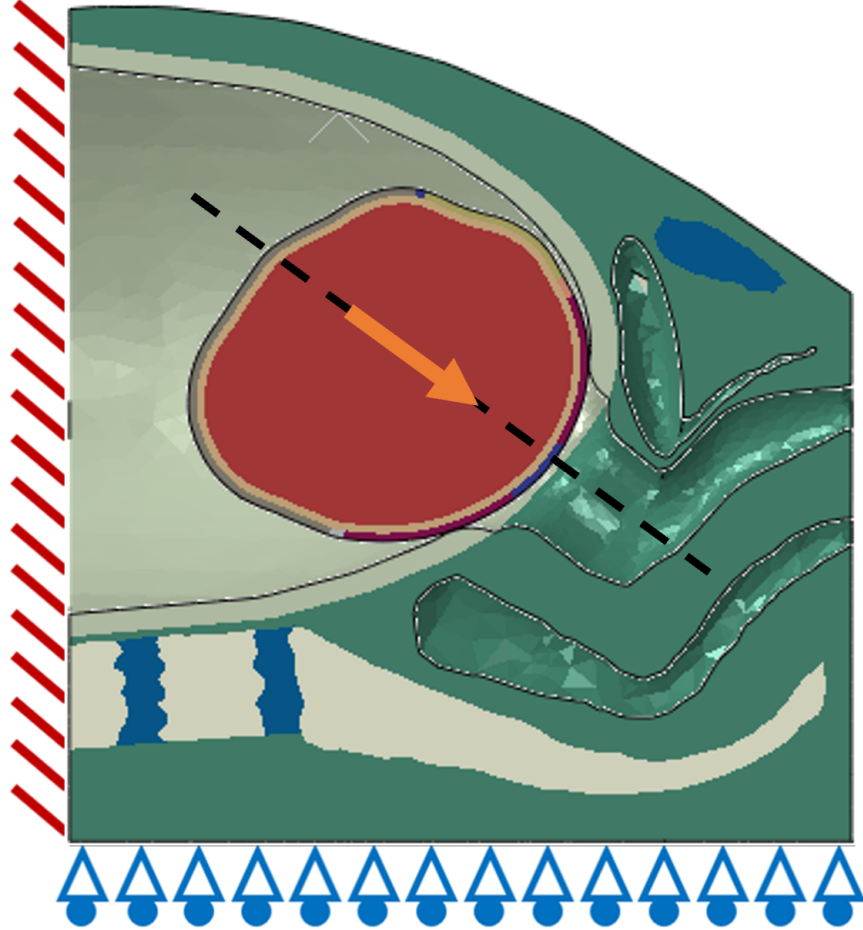


Figure 8: Sagittal view of the boundary (blue and red) and loading (orange) conditions for the birth simulation.

2.6. Molding Index

To quantify the molding in the fetal head models, a molding index (MI) [8], defined in Equation (1), was calculated at multiple points of fetal progression.

$$MI = \frac{MaVD^2}{BPD \times SOBD} \quad (1)$$

238 where MaVD, BPD, and SOBD are the maxillovertical, biparietal, suboccipi-
 239 tobregmatic diameters, respectively, see Figure 9a. An increase in MI indicates
 240 molding in a sugar-loaf shape [8]. These diameters were calculated by measuring
 241 the distance between nodes on the fetal head and tracking their displacements
 242 during fetal descent. The MaVD, the distance between the maxilla on the jaw
 243 to the vertex of the skull, had to be measured from a node on the model and ar-
 244 tificially extended during post processing to the diameter on the original model,
 245 as the simplified fetal head model does not have a jaw. This artificial extension
 246 is also shown in Figure 9a.

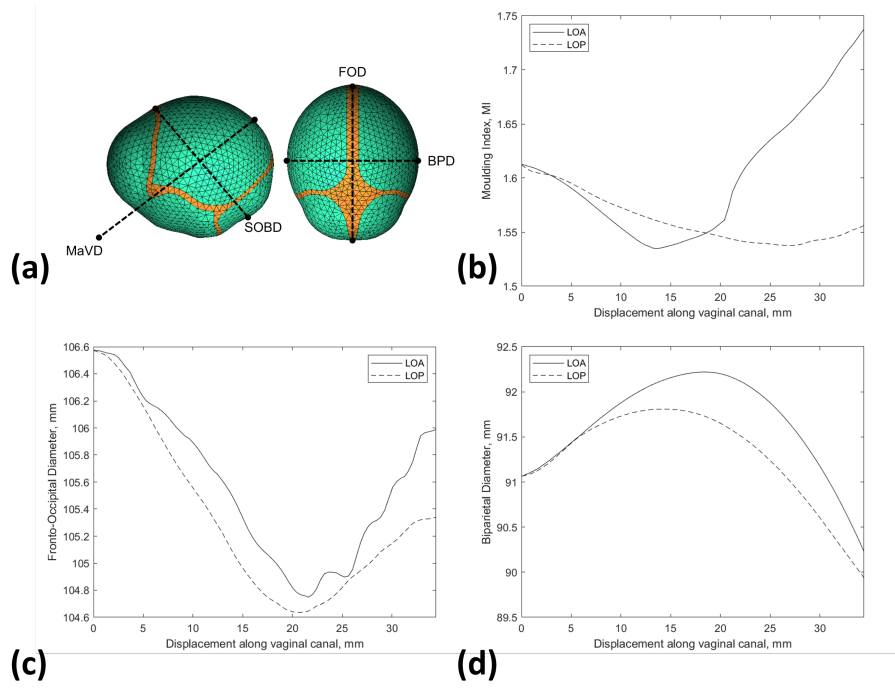


Figure 9: (a) Fetal diameters used to calculate the MI, (b) Evolution of the MI, (c) FOD, and
 (d) BPD with fetal descent for the LOA and LOP position simulations.

247 **3. Results**

248 Both simulations were able to progress up to around 34.4 mm into the canal.
249 The simulations stopped due to the distortion of suture elements from the fetal
250 head molding and suture folding. The displacement of the fetal head into the
251 canal for the LOA model is shown in an overlay plot in Figure 10. The dis-
252 placement along the canal was also calculated in terms of fetal station using the
253 ischial planes, see Figure 11; both descents began at -4 station and stopped at
254 -2 station.

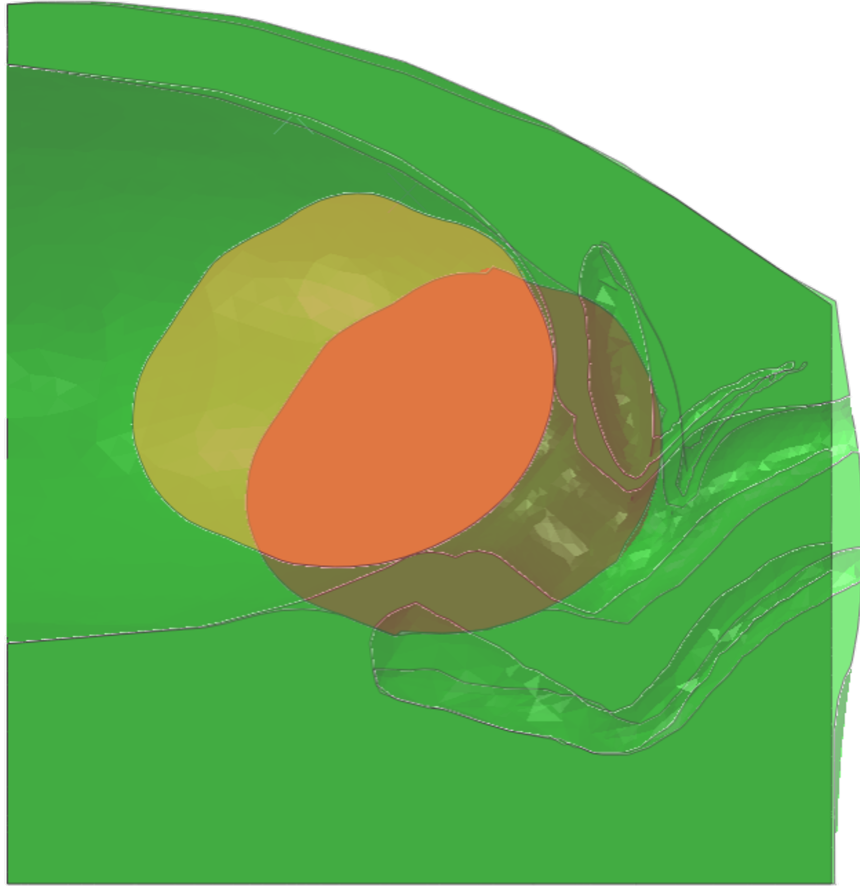


Figure 10: Overlay of the sagittal view of the LOA positioned fetus simulation at 0 mm and 34.4 mm fetal decent, green: maternal model and orange: fetal model.

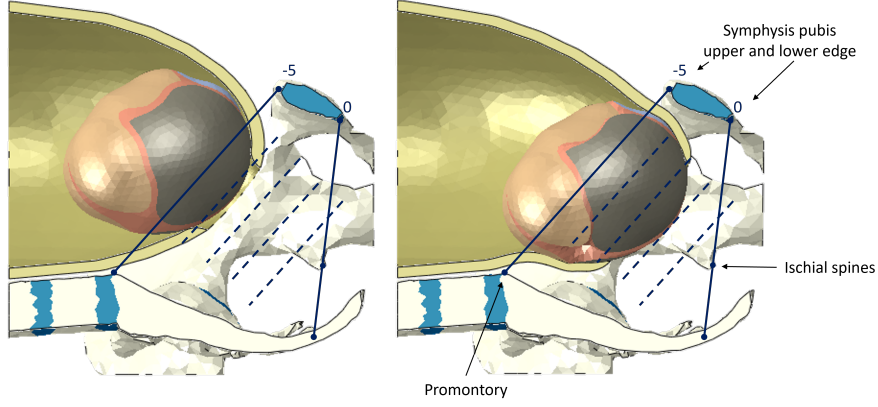


Figure 11: Sagittal view of the station of the LOA positioned fetal head before and at the end of the simulation, calculated from the ischial planes, here shown blue solid and dashed lines for station -5 to 0.

Progression of the fetus is described by fetal descent and defined here as displacement along the vaginal canal central axis. In addition to MI, BPD and FOD were also calculated, also shown in Figure 9a.

The initial and final MI, BPD, and FOD are listed in Table 3 and their change with fetal descent shown in Figure 9b-d.

Table 3: Initial and final fetal head MI and diameters.

	Initial	Final	
		LOA	LOP
MI	1.61	1.74	1.55
BPD	91.06 mm	90.23 mm	89.93 mm
FOD	106.57 mm	105.99 mm	105.34 mm

To compare the compression of the brain during the two cases, stress in the brain was measured at multiple points of fetal progression. The maximum von Mises stress and pressure were extracted from the brain elements, see Figures 12 and 13.

264 The maximum von Mises stress and absolute pressure experienced by each
265 fetal brain increased with progression, and reached maximum value at the end
266 of the simulation (34.4 mm of fetal descent): peak maximum von Mises stresses
267 of 0.7845 kPa and 0.5928 kPa, for the LOA and LOP simulations, respectively,
268 and peak maximum pressures of 0.5194 kPa and 0.4387 kPa, for the LOA and
269 LOP simulations, respectively.

270 In both models, the stress in the brain is concentrated around the areas of
271 the brain underneath the sutures (Figure 14), with the highest values under the
272 right coronal and sagittal sutures in both cases, and the anterior fontanelle and
273 occipitomastoid suture in the LOA positioned fetus.

274 The overlap of the sutures was evaluated through visualization of the fetal
275 head deformation. In the LOA positioned fetus, the beginning of overlap was
276 observed along both coronal, the occipitomastoid, and the lambdoid sutures
277 near the posterior fontanelle. The parietal bones encroached on each other and
278 had very slight overlap near the posterior fontanelle. The anterior fontanelle
279 also deformed inwards. In the LOP positioned fetus, the beginning of overlap
280 was observed along the coronal, right squamous, sagittal, and left lambdoid
281 suture with the anterior fontanelle bulging.

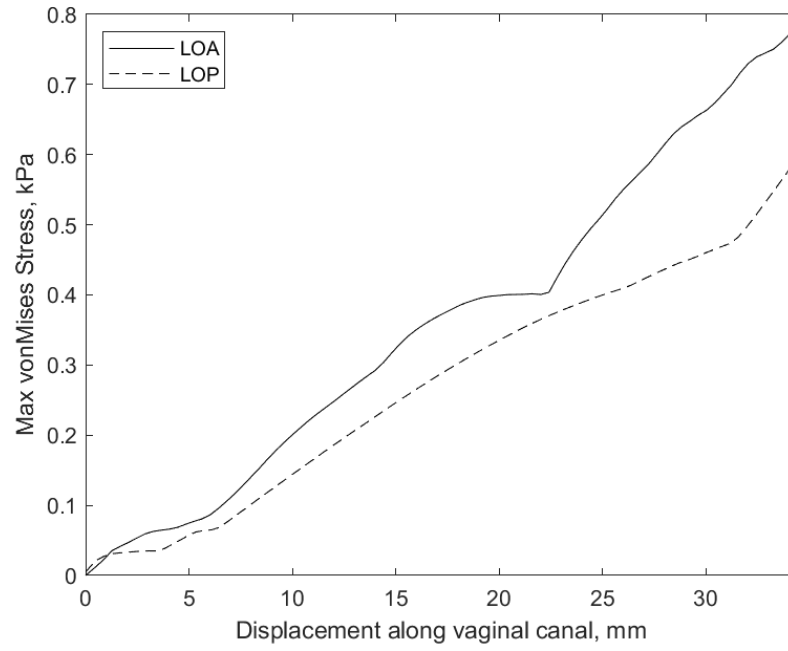


Figure 12: Evolution of maximum von Mises stress in the brain.

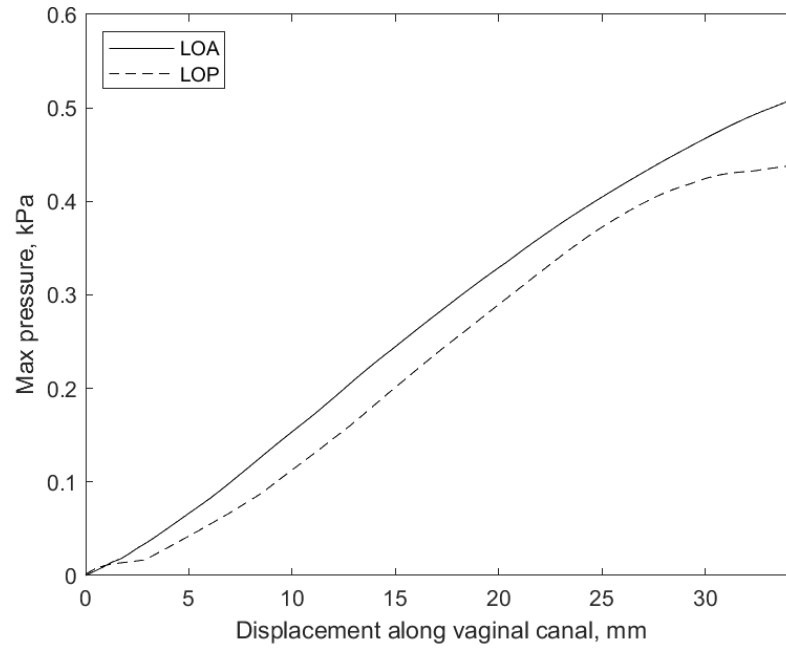


Figure 13: Evolution of maximum von Mises stress in the brain.

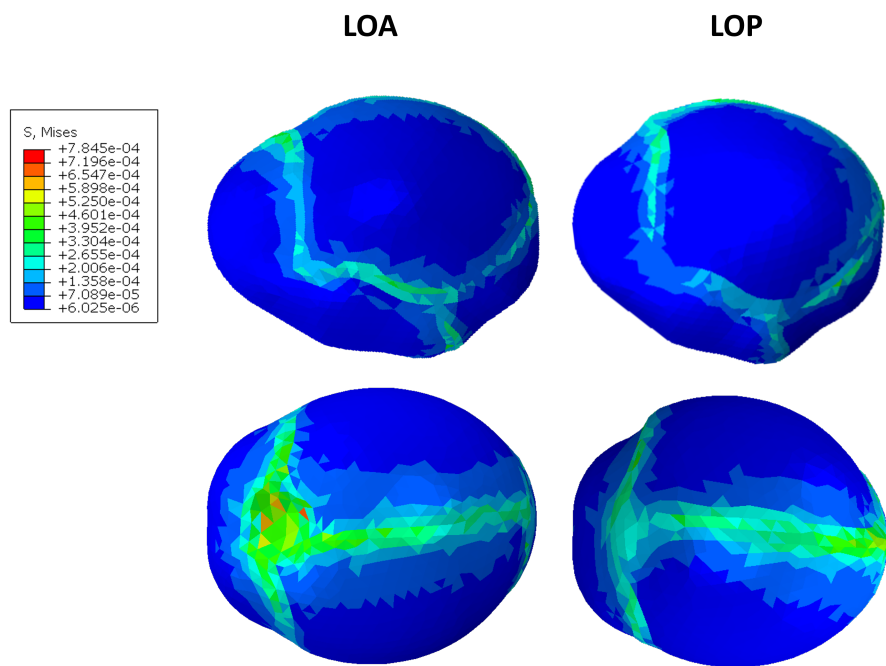


Figure 14: Sagittal view of the von Mises (MPa) distribution in the fetal brain, at 34.4 mm descent.

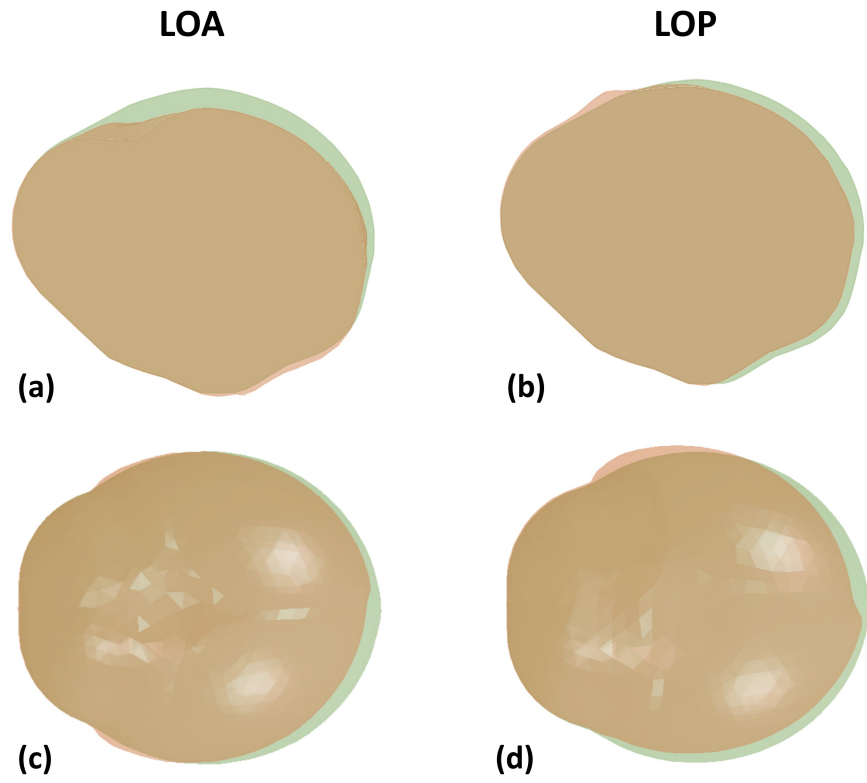


Figure 15: Sagittal cross-sectional, (a) and (b), and superior (c) and (d), view of the change in shape of the fetal brain for the LOA and LOP cases, at 34.4 mm descent. Green: initial brain shape before labour, Orange: brain shape during labour.

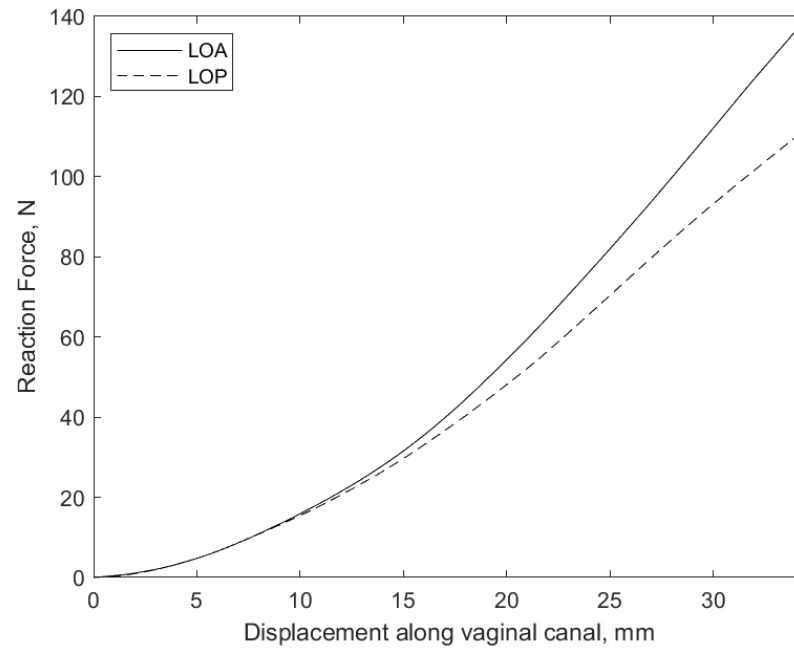


Figure 16: Evolution of the fetal head reaction force.

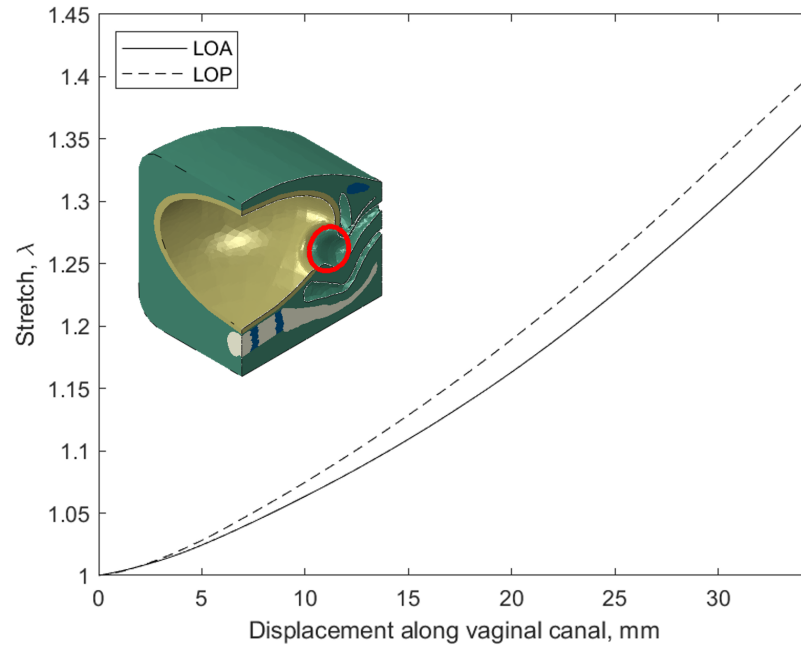


Figure 17: Evolution of the stretch of the external os of the cervix, calculated from a ring of nodes.

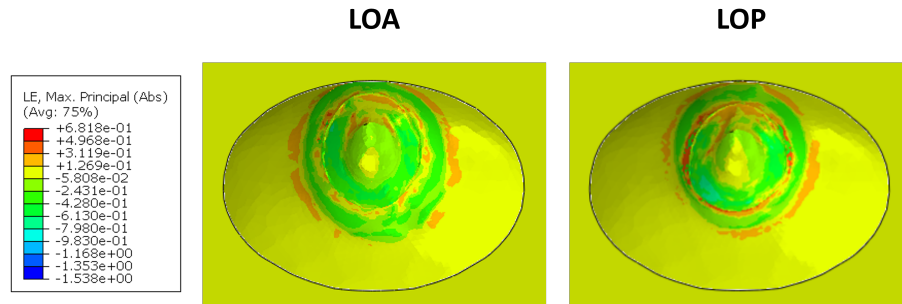


Figure 18: View, along the displacement axis, of the logarithmic strain of the maternal soft tissues at 34.4 mm descent.

283 reaction force required to displace the fetal head was measured at several points
284 of fetal progression (Figure 16). For both positions, the reaction force increased
285 with descent with the LOA positioned fetus experiencing higher reaction force.
286 Peak reaction forces of 136.94 N and 111.64 N were reached at the end of the
287 simulation for the LOA and LOP cases, respectively.

288 Our maternal model does not contain pelvic floor muscles, the stretch of
289 which are typically analysed to determine damage. Instead, to measure maternal
290 stretch, the displacement of a ring of nodes at the external os (or ostium of
291 uterus) of the cervix, see Figure 17, was measured and then used to calculate the
292 stretch of the maternal tissues. The distribution of maternal soft tissue strain
293 was also evaluated through visualization, shown at the end of fetal descent in
294 Figure 18. Uterine opening stretch increased with fetal descent with higher
295 stretch occurring in the LOP simulation, see Figure 17. Peak stretches of 1.37
296 and 1.40 were reached at the point the simulation stopped, for the LOA and
297 LOP cases, respectively.

298 Finally, peak stress and strain in the uterus were compared to and found to
299 be within the physiological range measured by Manoogian et al. [48].

300 4. Discussion

301 While computational models aimed at simulating birth have already been
302 proposed [19, 53, 54, 55, 56, 47], few have investigated specifically the forces
303 and deformations experienced by the fetal head during labour [19, 17, 18, 53].
304 This is due to both the difficulty in obtaining pediatric head geometry data
305 and the paucity of corresponding material response data at appropriate strain
306 rates. Previous models have used other pediatric soft tissue material property
307 data (e.g., dura for suture) and built models from skull replicas [17, 18]. These
308 have focused on the deformation and stress experienced by the skull and either
309 excluded the brain completely or did not investigate the loading of the brain.
310 The present study, however, proposes a comprehensive in silico model including
311 a maternal model and fetal head with brain and CSF to investigate the stresses

312 experienced by the fetal brain during the onset of the second phase of labour.
313 Two numerical simulations with a deformable fetal head were performed, with
314 the fetus in the left occiput anterior (LOA) and left occiput posterior (LOP)
315 position.

316 The simulations only progressed to 34.4 mm along the canal (~ 28 mm
317 vertically). This is less than the level of progression that peak stretches of the
318 pelvic floor have been simulated to occur ($\gtrsim 60$ mm vertically) [19, 20, 21, 53,
319 57]. Therefore, all peak values reported here are for the onset of the second
320 stage and may not be peak values for the complete second stage of labour.

321 Fetal station was calculated by plotting the ischial planes as described in
322 Obstetric Interventions [58]. The fetus starts quite high up in the pelvis (station
323 -4) which is higher than Moura et al.'s simulation but not unusual for a primipara
324 labour [19]. The pelvis was positioned within the maternal soft tissues using late
325 gestation MRIs as a reference. At the end of the third trimester, as the body
326 prepares itself for labour, the fetus settles, or drops lower, into the mother's
327 pelvis. The MRIs used are from late gestation females but not immediately
328 before labour, this would explain the higher station in our models as the fetus
329 could maybe drop further before labour.

330 Counterintuitively, the MI initially decreases, as shown in Figure 9. This
331 means the fetal head is molding in the opposite direction to that described by
332 Sorbe and Dahlgren [8]. After further progression of both fetal heads, the MIs
333 increase. After 34.4 mm of descent, only the LOA head has a higher MI than
334 initially; it is therefore deforming, as observed in Ref. [8], into the sugar loaf
335 shape. However, the LOP head has a lower MI at 34.4 mm than the head
336 pre-second stage of labour, driven by the lack of decrease in the SOBD. This
337 is most likely due to the SOBD not being the presenting diameter in the LOP
338 head as opposed to the LOA head. Sorbe and Dahlgren compared the change in
339 fetal head shape during labour by calculating the MI immediately post-partum
340 (molded/after labour) and 3-day post-partum (unmolded/before labour). In
341 OA-positioned fetuses, they reported a mean MI before labour of 1.61 (S.D
342 0.12) and after labour of 1.70 (S.D 0.16), and in OP-positioned fetuses, 1.47

343 (S.D 0.15) and 1.55 (S.D 0.06). We observed MIs before labour of 1.61 in both
 344 heads and after labour 1.74 and 1.55 for the LOA and LOP positioned head,
 345 respectively. These show strong agreement with the results reported by Sorbe
 346 and Dahlgren, including that fetuses positioned OP experience less molding (in
 347 the sugar-loaf shape). The approach of Sorbe and Dahlgren to use 3-day post-
 348 partum as the unmolded head before labour should be considered carefully as
 349 the resolution of molding after labour may not be “back” to the unmolded head
 350 shape in-utero before labour. Moura et al. also saw an increase in MI for both
 351 fetal positions with LOP experiencing a slightly lower MI [19]. Of note, our
 352 simulations were stopped relatively in labour, but those results might indicate
 353 that most of the deformation might have thus already happened at that stage.

354 Our model displayed an initial increase in BPD before a reduction in BPD
 355 to below the initial value, in both LOA and LOP, and an initial decrease in
 356 FOD before an increase (still below initial value) for both LOA and LOP. We
 357 anticipated either a decrease in BPD and FOD, as observed by Ami et al., or
 358 no change, as observed by Sorbe and Dahlgren [5, 8]. Ami et al. recorded
 359 the second stage of labour in open MRI and created 3D vector reconstructions
 360 of the fetal head from said MRI images [5]. This allowed for the study of
 361 the movement of the bony plates, change in brain shape, and change in head
 362 diameters during labour. They observed a median reduction in BPD and FOD
 363 of 2.28 and 11.64 mm, at higher values of reduction than in our FE models
 364 but they only measured fetal head molding at a single point of fetal progression
 365 and at a further descent into the canal; thus further progression of the model
 366 would be required for a proper comparison [5]. However, the change of BPD at
 367 this stage agrees with the trend in results of Moura et al.’s findings where an
 368 initial increase in BPD and then a sharp decrease to a diameter smaller than
 369 the initial BPD were observed. They also observed an initial decrease in FOD,
 370 eventually almost recovering its initial diameter [19]. This initial reduction in
 371 MI and increases in BPD and FOD are most likely due to the fact that, before
 372 the fetal head enters the vaginal canal, it is pushing on the entrance to the
 373 canal. This leads to the compacting of the head before it progresses further into

374 the canal where it experiences more circumferential compressive forces and can
375 then elongate before finally being expelled.

376 During the simulated second phase of labour, maximum von Mises stress
377 and absolute pressure in the fetal brain are higher in the fetus positioned LOA.
378 The nonlinear nature of the curves arises from the maximum von Mises be-
379 ing calculated from an envelope of the elements in the fetal brain, for which
380 the location of maximum stress may change with each time step. This higher
381 von Mises stress in the brain is also evident when observing the distribution of
382 stress in the brain in Figures 14. There is a larger area of brain under stress
383 in the LOA brain. The type of loading sustained in LOA is causing a wider
384 distribution and larger stresses in the brain. Stress is concentrated in areas of
385 the brain under the sutures in both presentations, as expected as the sutures
386 are deforming significantly. Notably, the stress is not concentrated in the ar-
387 eas of the brain underneath where the skull is in contact with the maternal
388 soft tissues or where the jaw is pushing (occiput and frontal). This suggests
389 that the deformable nature of the fetal skull with its sutures and the CSF layer
390 are collabouratively redistributing the loading on the fetal brain, in particular
391 sparing the heavily vascularized occipital region. The difference in brain defor-
392 mation between the two presentations is observable in Figure 14. The brain in
393 the LOA-presenting fetus is compressed in the MaVD direction with inversion
394 of the anterior fontanelle, while being compressed in the FOD direction with a
395 bulge in the anterior fontanelle for the LOP case. The LOA also experiences
396 more left side compression compared to LOP which has more right side com-
397 pression. These observations demonstrate that the fetal presentation (LOA vs.
398 LOP) significantly affect the type of fetal head deformation that occurs during
399 labour.

400 For both heads, there was very little displacement and movement of the
401 frontal bones and, as a result, no change or overlap in the frontal suture. This
402 differs from Ami et. al. who observed closing of the frontal suture in most cases
403 and overlap in 2/7 cases. However, both LOA and LOP fetal heads demon-
404 strated large movement of the parietal and occipital bones with the beginning

405 of an overlap at the coronal and lambdoid, along with the occipitomastoid and
 406 squamous sutures, and closing of the sagittal suture. This agrees with Ami et.
 407 al. who observed overlap of the coronal suture in 6/7 and in all cases for the
 408 lambdoid sutures. They also saw less overlap of the sagittal suture (2/7) agree-
 409 ing with our observations. In both models, the posterior fontanelle decreased in
 410 size agreeing with Ami et. al.'s observation whereas the anterior fontanelle did
 411 not decrease significantly in size, disagreeing with their observations. Overall
 412 this molding and movement mostly agreed with Ami et. al.'s observations across
 413 their seven participants: the LOA and LOP positioned fetal heads underwent
 414 different molding with overlap of sutures in different locations and different cra-
 415 nial bone relative displacements, which is most likely due to the different area
 416 of the pelvis and vaginal canal that each cranial bone is interacting with in each
 417 position.

418 Peak reactions for LOA and LOP positioned fetuses were 136.94 N and
 419 111.64 N, respectively, which shows good agreement with the estimated expul-
 420 sion force of ~ 120 N calculated by Ashton-Miller and DeLancey [59]. It was
 421 anticipated that the LOP presenting fetus would have higher expulsion force as
 422 Moura et. al. found that occiput posterior presentation is more favorable for
 423 the fetus and causes higher stress in the pelvic floor than anterior presenting,
 424 but the opposite was found in terms of maternal effort. A possible explanation
 425 for this could be the narrower canal opening is causing more expulsive effort to
 426 displace the head as more molding is required and this is more favorable to the
 427 mother as there is, still at this stage, less stretch of the lower uterus and vaginal
 428 canal. Other considerations explaining the potential discrepancy include the
 429 contributions of lateral forces vs. longitudinal forces.

430 There was also a difference in stretch of the uterus/canal opening. In both
 431 cases, the uterus opening widened as the fetus descended, as expected, but with
 432 LOP causing a slightly higher stretch of the external os. In this study, the
 433 maximum stretch reached around 1.4. Note that this value is not representative
 434 of peak stretch for the full expulsion of the fetus (it is solely for the onset of the
 435 second stage). With further progression of the fetal head in our model along

436 with the consideration of the current trend observed in our results, maternal
 437 tissue stretch would thus be anticipated to continue to increase for some time
 438 before plateauing. This maximum stretch was similar to the 1.63 observed by
 439 Moura et al. but they calculated this for the lower pelvic floor muscles and not
 440 the external os [19]. This pattern of stretch in LOA and LOP is visible in Figure
 441 18, with LOP having a more concentrated and higher strain in the maternal soft
 442 tissue. The upper uterine segment is predominantly undergoing stretch in the
 443 superior-inferior direction, the lower uterine segment thinning and compressing,
 444 and the cervix experiencing circumferential stretch. The slightly higher stretch
 445 and the low stresses in the fetal head agrees with Moura et al.'s findings that
 446 the occiput posterior presentation is more favorable for the fetus [19]. This
 447 indicates that labour is a balance between deformation and stress in mother
 448 and baby, and that indeed something "has to give" on both sides. As typically
 449 fetuses have little to no consequences from the labour process, maybe the fetal
 450 anatomy and physiology is better developed to deal with deformation than the
 451 maternal side while positions that reduce stress on the fetus, such as LOP, do
 452 cause other issues such as overstretch of the pelvic floor or an obstructed labour.

453 There are limitations to our model: both the maternal and fetal models are
 454 simplified FE models that aim to capture the key features and reduce compu-
 455 tational cost but at the loss of detailed features. The focus of this study is
 456 the deformation and stress on the fetal brain; this simplified fetal head model
 457 has a smooth brain that does not distinguish between brainstem, ventricles,
 458 grey and white matter, etc. This simplification allows for the investigation of
 459 the overall and general locations of stress in the fetal brain during labour, not
 460 previously reported in the literature, to the best of our knowledge, at a lower
 461 computational cost. However, for further investigation into potential mecha-
 462 nisms of injury, a more detailed brain is needed to explore how the difference in
 463 mechanical properties of the regions of the brain interact with each other. One
 464 issue encountered when creating the fetal head model was suture overlap, which
 465 was the reason the simulation could not progress any further, i.e. the overlap
 466 of cranial bones causes extreme distortion of elements. It was only possible to

467 observe the beginning of this overlap before elements became distorted. Due to
 468 the paucity of research into the mechanical behavior of neonatal tissues, sev-
 469 eral approximations and assumptions were made. As further research appears,
 470 these first approximations should be revised. Again, as the focus of this study
 471 is on the fetal head, the simplified maternal model does not include pelvic floor
 472 muscles, the tissues that most commonly sustain trauma and damage during
 473 labour. For further investigations into maternal injury, these tissues will need
 474 to be included in the model. The maternal pelvis is also from a different patient
 475 than the simplified soft tissues and both unrelated to the fetal model. There-
 476 fore, it is possible that these combination of patients does not pose a plausible
 477 successful vaginal delivery scenario. However, combining these geometries al-
 478 lows for a more realistic approximation of maternal labour and its boundary
 479 conditions than without. The second stage of labour is a dynamic scenario with
 480 contractions and relaxation of the uterus. This paper uses a static approach
 481 due to the complexities of the problem and lack of research into the viscoelastic
 482 properties of neonatal tissues. The next progression of these models would be
 483 to incorporate these dynamic aspects.

484 **5. Conclusion**

485 This paper presents a FE model of fetal head and maternal anatomy for sim-
 486 ulating the onset of the second stage of labour. Simulating two fetal positions,
 487 left-occiput-anterior and left-occiput-posterior, enabled the comparison of two
 488 cases of stress in the brain, which has not been previously investigated during
 489 labour.

490 The results indicate that the highest levels of stress in the brain occur at the
 491 sutures. This is where the most important deformation occurs in the skull and
 492 where the forces on the skull (then transmitted on to the brain) are highest.
 493 The results also indicate that position effects the level and location of stress
 494 and deformation in the fetal brain. Posterior position causes lower stress in the
 495 fetal brain but higher stretch in the maternal tissues, suggesting that posterior

position is more favorable for the fetus and anterior position for the mother. Further progression of the fetus is needed to validate this. It is worth emphasizing that, while clinical studies have already indicated what parameters influence a successful birth for mother (gestational age, fetal position, gravidity, and maternal age), there is still a paucity of research on the fetal brain in this stage of labour and the model could not be validated against clinical data. Future work shall focus on the parametrization of the model to determine what factors most greatly impact fetal brain stress during labour.

6. Acknowledgments

The authors thank Divya Rajasekharan for her work on segmenting the pelvic bone from MRI and acknowledge support from the EPSRC IAA grant that facilitated the collaboration between Oxford and Columbia University. This work in part is sponsored by the Eunice Kennedy Shriver Institute of Child Health and Human Development under Award R01HD091153. The content is solely the responsibility of the authors and does not necessarily represent the official views of the National Institutes of Health. AC also acknowledges support from EPSRC doctoral training funding.

513 References

- 514 [1] R. Warren, S. Arulkumaran (Eds.), Best Practice in Labour and Delivery,
515 1st Edition, Cambridge University Press, Cambridge, 2009, Ch. 1: Pelvic
516 and fetal cranial anatomy and mechanism of labour, pp. 1–13.
- 517 [2] L. Lindgren, The causes of foetal head moulding in labour, *Acta. Obstet.*
518 *Gynecol. Scand.* 39 (1) (1960) 46–62. doi:10.3109/00016346009157836.
- 519 [3] J. Baxter, Moulding of the foetal head, *J. Obstet. Gynaecol. Brit. Emp.*
520 53 (3) (1946) 212–218. doi:10.1111/j.1471-0528.1946.tb03903.x.
- 521 [4] N. N. Rabelo, H. Matushita, D. D. Cardeal, Traumatic brain lesions in
522 newborns, *Arquivos de Neuro-Psiquiatria* 75 (3) (2017) 180–188. doi:
523 10.1590/0004-282X20170016.
- 524 [5] O. Ami, J. C. Maran, P. Gabor, E. B. Whitacre, D. Musset, C. Dubray,
525 G. Mage, L. Boyer, Three-dimensional magnetic resonance imaging of foetal
526 head moulding and brain shape changes during the second stage of labour,
527 *PLoS ONE* 14 (5) (2019) e0215721. doi:10.1371/journal.pone.0215721.
- 528 [6] F. G. Cunningham, K. J. Leveno, S. L. Bloom, C. Y. Spong, J. S. Dashe,
529 B. L. Hoffman, B. M. Casey, J. S. Sheffield (Eds.), *Williams Obstetrics*,
530 24th Edition, McGraw-Hill Education/Medical, New York, 2014.
- 531 [7] T. F. Baskett, V. M. Allen, C. M. O’Connell, A. C. Allen, Fetal trauma in
532 term pregnancy, *American Journal of Obstetrics and Gynecology* 197 (5)
533 (2006) 499.e1–499.e7. doi:10.1016/j.ajog.2007.03.065.
- 534 [8] B. Sorbe, S. Dahlgren, Some important factors in the moulding of the
535 foetal head during vaginal delivery - a photographic study, *Int. J. Gynaecol.*
536 *Obstet.* 21 (3) (1983) 205–212. doi:10.1016/0020-7292(83)90081-4.
- 537 [9] A. Chaturvedi, A. Chaturvedi, A. L. Stanescu, J. G. Blickman, S. P.
538 Meyers, Mechanical birth-related trauma to the neonate: An imag-
539 ing perspective, *Insights Imaging* 9 (1) (2018) 103–118. doi:10.1007/
540 s13244-017-0586-x.

- [10] A. H. DeCherney, L. Nathan, N. Laufer, A. S. Roman, 12th Edition, McGraw-Hill Education, New York, NY, 2019.
- [11] K. P. Hanretty, I. Ramsden, R. Callander, 7th Edition, Churchill Livingstone Wordmark, Edinburgh, 2010.
- [12] S. Akmal, E. Tsoi, R. Howard, E. Osei, K. H. Nicolaides, Investigation of occiput posterior delivery by intrapartum sonography, *Ultrasound Obstet Gynecol* 24 (2004) 425–428. doi:10.1002/uog.1064.
- [13] J. Senecal, X. Xiong, W. D. Fraser, Effect of fetal position on second-stage duration and labor outcome, *Obstetrics and Gynecology* 105 (4) (2005) 763–772. doi:10.1097/01.AOG.0000154889.47063.84.
- [14] Y. W. Cheng, B. L. Shaffer, A. B. Caughey, The association between persistent occiput posterior position and neonatal outcomes, *Obstetrics and Gynecology* 107 (4) (2006) 837–844. doi:10.1097/01.AOG.0000206217.07883.a2.
- [15] H. H. Foggin, A. Y. Albert, N. C. Minielly, S. Lisonkova, N. A. Koenig, E. N. Jacobs, G. W. Cundiff, Labor and delivery outcomes by delivery method in term deliveries in occiput posterior position: a population-based retrospective cohort study, *AJOG Global Reports* 2 (4) (2022) 100080. doi:10.1016/j.xagr.2022.100080.
- [16] G. K. McPherson, T. J. Kriewall, Foetal head moulding: An investigation utilising a finite element model of the foetal parietal bone, *Journal of Biomechanics* 13 (1) (1980) 17–26. doi:10.1016/0021-9290(80)90004-4.
- [17] R. J. Lapeer, R. W. Prager, Fetal head moulding: finite element analysis of a fetal skull subjected to uterine pressures during the first stage of labour, *Journal of Biomechanics* 34 (9) (2001) 1125–1133. doi:10.1016/S0021-9290(01)00070-7.

- 567 [18] F. Pu, L. Xu, D. Li, S. Li, L. Sun, L. Wang, Y. Fan, Effect of different
568 labor forces on fetal skull moulding, *Medical Engineering and Physics* 33 (5)
569 (2011) 620–625. doi:10.1016/j.medengphy.2010.12.018.
- 570 [19] R. Moura, M. Borges, D. A. Oliveira, M. P. L. Parente, N. Kimmich,
571 T. Mascarenhas, R. M. Natal, A biomechanical study of the birth position:
572 a natural struggle between mother and fetus, *Biomech Model Mechanobiol*
573 21 (2022) 937–951. doi:10.1007/s10237-022-01569-2.
- 574 [20] M. Borges, R. Moura, D. Oliveira, M. Parente, T. Mascarenhas, R. Natal,
575 Effect of the birthing position on its evolution from a biomechanical point of
576 view, *Computer Methods and Programs in Biomedicine* 200 (2021) 105921.
577 doi:10.1016/j.cmpb.2020.105921.
- 578 [21] R. Moura, M. Borges, M. C. P. V. Pouca, D. A. Oliveira, M. P. L. Parente,
579 N. Kimmich, T. Mascarenhas, R. M. Natal, A numerical study on fetal
580 head molding during labor, *Int J Numer Meth Biomed Engng.* 37 (1) (2020)
581 e3411. doi:10.1002/cnm.3411.
- 582 [22] K. D. Heyborne, A systematic review of intrapartum fetal head compres-
583 sion: What is the impact on the fetal brain?, *AJP Rep.* 7 (2) (2017) e79–e85.
584 doi:10.1055/s-0037-1602658.
- 585 [23] G. A. Khalid, R. K. Prahuc, O. Arthurs, M. D. Jones, A coupled physical-
586 computational methodology for the investigation of short fall related in-
587 fant head impact injury, *Forensic Science International* 300 (2019) 170–186.
588 doi:10.1016/j.forsciint.2019.04.034.
- 589 [24] G. A. Khalid, A coupled physical–computational methodology for the
590 investigation of short fall related infant head impact, Ph.D. thesis, Cardiff
591 University (2018).
592 URL [https://orca.cardiff.ac.uk/id/eprint/117559/1/](https://orca.cardiff.ac.uk/id/eprint/117559/1/2018KhalidGAPhD.pdf)
593 [2018KhalidGAPhD.pdf](https://orca.cardiff.ac.uk/id/eprint/117559/1/2018KhalidGAPhD.pdf)

- 594 [25] W. H. Organization, Who child growth standards, head circumference
595 (2006).
596 URL [https://www.who.int/tools/child-growth-standards/
597 standards/head-circumference-for-age](https://www.who.int/tools/child-growth-standards/standards/head-circumference-for-age)
- 598 [26] T. Kiserud, G. Piaggio, G. Carroli, M. Widmer, J. Carvalho, L. N. Jensen,
599 D. Giordano, J. G. Cecatti, The world health organization fetal growth
600 charts: A multinational longitudinal study of ultrasound biometric mea-
601 surements and estimated fetal weight, *PLoS Med.* 14 (1) (2017) e1002220.
602 doi:10.1371/journal.pmed.1002220.
- 603 [27] P. Cignoni, M. Callieri, M. Corsini, M. Dellepiane, F. Ganovelli,
604 G. Ranzuglia, MeshLab: an Open-Source Mesh Processing Tool, in:
605 V. Scarano, R. D. Chiara, U. Erra (Eds.), *Eurographics Italian Chap-
606 ter Conference, The Eurographics Association, 2008.* doi:10.2312/
607 LocalChapterEvents/ItalChap/ItalianChapConf2008/129-136.
- 608 [28] P. Cignoni, C. Rocchini, R. Scopigno, Metro: measuring error on simplified
609 surfaces, in: *Computer Graphics Forum, Vol. 17, Blackwell Publishers,*
610 1998, pp. 167–174.
- 611 [29] A. R. Westervelt, M. Fernandez, M. House, J. Vink, C.-L. Nhan-Chang,
612 R. Wapner, K. M. Myers, A parameterised ultrasound-based finite element
613 analysis of the mechanical environment of pregnancy, *Journal of Biomedical
614 Engineering* 139 (5) (2011) 051004 (11 pages). doi:10.1115/1.4036259.
- 615 [30] G. D. Bryant-Greenwood, The extracellular matrix of the human fe-
616 tal membranes: Structure and function, *Placenta* 19 (1) (1998) 1–11.
617 doi:10.1016/S0143-4004(98)90092-3.
- 618 [31] A. Baah-Dwomoh, J. McGuire, T. Tan, R. DeVita, Mechanical properties
619 of female reproductive organs and supporting connective tissues: A review
620 of the current state of knowledge, *Applied Mechanics Reviews* 68 (6) (2016)
621 060801 (12 pages). doi:10.1115/1.4034442.

- [32] J. Luo, C. Betschart, J. A. Ashton-Miller, J. O. L. DeLancey, Quantitative analyses of variability in normal vaginal shape and dimension on mr images, *Int Urogynecol J* 27 (2016) 1087–1095. doi:10.1007/s00192-016-2949-0.
- [33] K. T. Barnhart, A. Izquierdo, E. S. Pretorius, D. M. Shera, M. Shabbout, A. Shaunik, Baseline dimensions of the human vagina, *Human Reproduction* 21 (6) (2006) 1618–1622. doi:10.1093/humrep/de1022.
- [34] S. H. Zhou, I. D. McCarthy, A. H. McGregor, R. R. H. Coombs, S. P. F. Hughes, Geometrical dimensions of the lower lumbar vertebrae – analysis of data from digitised ct images, *Eur Spine J.* 9 (3) (2000) 242 – 248. doi:10.1007/s005860000140.
- [35] B. Coats, S. S. Margulies, Material properties of human infant skull and suture at high rates, *Journal of Neurotrauma* 23 (8) (2006) 1222–1232. doi:10.1089/neu.2006.23.1222.
- [36] X. Li, H. Sandler, S. Kleiven, The importance of nonlinear tissue modelling in finite element simulations of infant head impacts, *Biomech. Model Mechanobiol.* 16 (3) (2017) 823–840. doi:10.1007/s10237-016-0855-5.
- [37] G. K. McPherson, T. J. Kriewall, The elastic modulus of foetal cranial bone: A first step towards an understanding of the biomechanics of foetal head moulding, *J. Biomech.* 13 (1) (1980) 9–16. doi:10.1016/0021-9290(80)90003-2.
- [38] T. J. Kriewall, Structural, mechanical, and material properties of fetal cranial bone, *Am. J. Obstet. Gynecol.* 143 (6) (1982) 707–714. doi:0.1016/0002-9378(82)90119-3.
- [39] G. K. McPherson, T. J. Kriewall, A. C. Tsai, Bending properties and ash content of foetal cranial bone, *J. Biomech.* 14 (2) (1981) 73–79. doi:10.1016/0021-9290(81)90166-4.
- [40] S. Budday, T. C. Ovaert, G. A. Holzapfel, P. Steinmann, E. Kuhl, Fifty shades of brain: A review on the mechanical testing and modelling of brain

- tissue, *Archives of Computational Methods in Engineering* 27 (2020) 1187–1230. doi:10.1007/s11831-019-09352-w.
- [41] S. Chatelin, A. Constantinesco, R. Willinger, Fifty years of brain tissue mechanical testing: From in vitro to in vivo investigations, *Biorheology* 47 (2010) 255–276. doi:10.3233/BIR-2010-0576.
- [42] K. L. Thibault, S. S. Margulies, Age-dependent material properties of the porcine cerebrum: effect on paediatric inertial head injury criteria, *Journal of Biomechanics* 31 (12) (1998) 1119–1126. doi:10.1016/s0021-9290(98)00122-5.
- [43] M. T. Prange, S. S. Margulies, Regional, directional, and age-dependent properties of the brain undergoing large deformation, *J. Biomech. Eng.* 124 (2) (2002) 244–252. doi:10.1115/1.1449907.
- [44] J. Yeung, L. Jugé, A. Hatt, L. E. Bilston, Paediatric brain tissue properties measured with magnetic resonance elastography, *Biomechanics and Modeling in Mechanobiology* 18 (2019) 1497–1505. doi:10.1007/s10237-019-01157-x.
- [45] S. Roth, J. Raul, R. Willinger, Finite element modelling of paediatric head impact: Global validation against experimental data, *Comput. Methods Programs Biomed.* 99 (1) (2010) 25–33. doi:10.1016/j.cmpb.2009.10.004.
- [46] Z. Li, J. Hu, M. P. Reed, J. D. Rupp, C. N. Hoff, J. Zhang, B. Cheng, Development, validation, and application of a parametric pediatric head finite element model for impact simulations, *Ann. Biomed. Eng.* 39 (12) (2011) 2984–2997. doi:10.1007/s10439-011-0409-z.
- [47] R. Buttin, F. Zara, B. Shariat, T. Redarce, G. Grange, Biomechanical simulation of the foetal decent without imposed theoretical trajectory, *Computer methods and programs in biomedicine* 111 (2) (2013) 389–401. doi:10.1016/j.cmpb.2013.04.005.

- [48] S. J. Manoogian, J. A. Bisplinghoff, A. R. Kemper, S. M. Duma, Dynamic material properties of the pregnant human uterus, *J. Biomech.* 45 (9) (2012) 1724–1727. doi:10.1016/j.jbiomech.2012.04.001.
- [49] M. Ramezani, S. Klima, P. L. C. de la Herverie, J. Campo, J.-B. L. Joncour, C. Rouquette, M. Scholze, N. Hammer, In silico pelvis and sacroiliac joint motion: Refining a model of the human osteoligamentous pelvis for assessing physiological load deformation using an inverted validation approach, *BioMed Research International* 1 (2019) 1–12. doi:10.1155/2019/3973170.
- [50] G. J. Dakin, R. A. Arbelaez, F. J. M. IV, J. E. Alonso, K. A. Mann, A. W. Eberhardt, Elastic and viscoelastic properties of the human pubic symphysis joint: Effects of lateral impact loading, *ASME. J Biomech Eng.* 123 (3) (2001) 218–226. doi:10.1115/1.1372321.
- [51] A. M. Loyd, Studies of the human head from neonate to adult: An inertial, geometrical, and structural analysis with comparisons to the adult head, Ph.D. thesis, Duke University (2011).
URL <https://hdl.handle.net/10161/4986>
- [52] K. Nishijima, M. Yoneda, T. Hirai, K. Takakuwa, T. Enomoto, Biology of the vernix caseosa: A review, *J. Obstet. Gynaecol. Res.* 45 (11) (2019) 2145–2149. doi:10.1111/jog.14103.
- [53] M. E. T. Silva, D. A. Oliveira, T. H. Roza, S. B. ao, M. P. L. Parente, T. Mascarenhas, R. M. N. Jorge, Study on the influence of the fetus head molding on the biomechanical behavior of the pelvic floor muscles, during vaginal delivery, *Journal of Biomechanics* 48 (9) (2015) 1600–1605. doi:10.1016/j.jbiomech.2015.02.032.
- [54] M. C. P. V. Pouca, J. P. S. Ferreira, D. A. Oliveira, M. P. L. Parente, M. T. Mascarenhas, R. M. N. Jorge, Simulation of the uterine contractions and foetus expulsion using a chemo-mechanical constitutive

706 model, *Biomechanics and Modeling in Mechanobiology* 18 (2019) 829–843.
707 doi:10.1007/s10237-019-01117-5.

708 [55] M. R. Routzong, P. A. Moalli, S. Maiti, R. D. Vita, S. D. Abramowitch,
709 Novel simulations to determine the impact of superficial perineal structures
710 on vaginal delivery, *Interface Focus* 9 (2019) 20190011. doi:10.1098/rsfs.
711 2019.0011.

712 [56] R. Lapeer, Z. Gerikhanov, S. Sadulaev, V. Audinis, R. Rowland, K. Crozier,
713 E. Morris, A computer-based simulation of childbirth using the partial
714 dirichlet–neumann contact method with total lagrangian explicit dynamics
715 on the gpu, *Biomechanics and Modeling in Mechanobiology* 18 (2019) 681–
716 700. doi:10.1007/s10237-018-01109-x.

717 [57] K.-C. Lien, B. Mooney, J. O. L. DeLancey, J. A. Ashton-Miller, Levator ani
718 muscle stretch induced by simulated vaginal birth, *Obstet Gynecol* 103 (1)
719 (2004) 31–40. doi:10.1097/01.AOG.0000109207.22354.65.

720 [58] *Anatomy*, Cambridge University Press, 2017, pp. 1–16.

721 [59] J. Ashton-Miller, J. Delancey, On the biomechanics of vaginal birth and
722 common sequelae, *Annu Rev Biomed Eng.* 11 (2009) 163–176. doi:10.
723 1146/annurev-bioeng-061008-124823.